

PES and XAS Study on Electronic Structures of Multiferroic RMnO₃ (R=Y, Er)

J.-S. Kang^{*,1,2}, S. W. Han², J.-G. Park^{2,3}, S. C. Wi¹, S. S. Lee¹,
G. Kim¹, H. J. Song⁴, H. J. Shin⁴, W. Jo⁵, and B. I. Min⁶

¹*Department of Physics, The Catholic University of Korea, Puchon 420-743, Korea*

²*CSCMR, Seoul National University, Seoul 151-742, Korea*

³*Department of Physics, Sungkyunkwan University, Suwon 440-746, Korea*

⁴*Pohang Accelerator Laboratory (PAL), POSTECH, Pohang 790-784, Korea*

⁵*Department of Physics, Ewha Womans University, Seoul 120-750, Korea*

⁶*Department of Physics, POSTECH, Pohang 790-784, Korea*

(Dated: November 21, 2018)

Electronic structures of multiferroic RMnO₃ (R=Y, Er) have been investigated by employing photoemission spectroscopy (PES) and x-ray absorption spectroscopy (XAS). We have found that Mn ions in RMnO₃ are in the trivalent high-spin state with the total spin of $S = 2$. The occupied Mn ($d_{xz} - d_{yz}$) states lie deep below E_F , while the occupied Mn ($d_{xy} - d_{x^2-y^2}$) states overlap very much with the O $2p$ states. It is observed that the PES spectral intensity of Mn $3d$ states is negligible above the occupied O $2p$ bands, suggesting that YMnO₃ is likely to be a charge-transfer insulator. The Mn $d_{3z^2-r^2}$ state is mostly unoccupied in the ferroelectric phase of YMnO₃.

PACS numbers: 77.84.-s, 79.60.-i, 71.20.Eh

Hexagonal yttrium (Y) and rare-earth (R) manganites of the formula RMnO₃ (R=Ho, Er, Tm, Yb, Lu, or Y) belong to an interesting class, known as multiferroic materials, in which the ferroelectric and magnetic ordering coexist at low temperatures^{1,2,3,4}. Hexagonal RMnO₃ compounds have antiferromagnetic ordering with the Neel temperature (T_N) of $T_N < 70 - 130$ K^{1,5}, and the ferroelectric ordering occurs at a high temperature ($T_E \sim 600 - 990$ K)^{1,2}. RMnO₃ crystallizes in two structural phases; the hexagonal phase when the ionic radius of R is small, and the orthorhombic phase when the ionic radius of R is rather large. Note that the ferroelectric ordering occurs only in the hexagonal phase of RMnO₃, while the magnetic ordering occurs in both hexagonal and orthorhombic phases. In the hexagonal structure, each Mn ion is surrounded by three in-plane and two apical oxygen ions, and so it is subject to a trigonal crystal field⁶. These MnO₅ blocks are connected two-dimensionally through their corners, and the triangular lattice of Mn³⁺ ions is formed. These hexagonal RMnO₃ compounds experience characteristic distortions such as tilting of MnO₅ blocks and the displacement of R³⁺ ions along the c axis, causing a ferroelectric polarization^{6,7}.

There seems to be a strong coupling between the ferroelectric and magnetic ordering in hexagonal RMnO₃ compounds. For example, a critical change of dielectric constants at T_N has been reported for RMnO₃ polycrystalline samples^{8,9,10}, suggesting a coupling between the ferroelectric and magnetic ordering. Further, the coupled antiferromagnetic and ferroelectric domains have been observed in YMnO₃¹¹, and the magnetic phase of HoMnO₃ has been observed to be controlled by the electric field¹². In the optical study of LuMnO₃¹³, a strong coupling of antiferromagnetism to the optical absorption spectra has been observed.

Understanding the origin of the coexistence of magnetism and ferroelectricity in hexagonal RMnO₃ is a fun-

damental physics question, but has not been well understood yet. The d^0 -ness rule is generally accepted in ferroelectricity. That is, a ferroelectric displacement of B cation in ABO₃ is inhibited if the formal charge of B ion does not correspond to a d^0 electron configuration due to the strong on-site Coulomb interaction between d electrons. In contrast, the occupancy of transition-metal d electrons is crucial in the magnetic ordering. Thus the simultaneous magnetic and ferroelectric ordering in RMnO₃ seems to break the d^0 -ness rule. It was suggested that this multiferroic property is a result of the effective 1-dimensional (1-D) d^0 -ness along the c -axis^{14,15}. According to the electronic structure calculations^{16,17}, the Mn³⁺ ($3d^4$) ion in YMnO₃ is not a Jahn-Teller ion since the highest occupied $3d$ level ($d_{xy} - d_{x^2-y^2}$) is non-degenerate because of the trigonal symmetry of the surrounding oxygen ions. The $d_{3z^2-r^2}$ state is mostly unoccupied so that this effective 1-D d^0 orbital along the c -axis allows ferroelectricity to occur via the usual ligand-field stabilization mechanism. This is a plausible idea, but has not been confirmed experimentally yet.

In order to understand the origin of the multiferroicity in hexagonal RMnO₃, it is important to investigate the electronic structures of hexagonal RMnO₃, including the valence states of Mn ions, the character of the lowest unoccupied $3d$ states of the Mn ion below and above the ferroelectric transition. In principle, these investigations are possible by employing the polarization-dependent soft x-ray absorption spectroscopy (XAS) and valence-band photoemission spectroscopy (PES) measurements. PES and XAS are powerful experimental methods for providing direct information on the electronic structures of solids. In practice, however, these spectroscopic measurements are not easy for these multiferroic materials. Normally these systems are good insulators having wide band gaps, and so they are not good for electron spectroscopy studies. For the polarization-dependent experi-

ments, single crystals are prerequisite. Further, it is difficult to study the changes in the electronic structure across T_E using these spectroscopy experiments because it is practically not compatible with the ultra high vacuum required for the experiments to achieve these high temperatures ($T_E \sim 600 - 990$ K).

In this paper, we report the valence-band PES, O $1s$ XAS, and Mn $2p$ XAS study of polycrystalline RMnO_3 ($R=Y, \text{Er}$) samples at room temperature which belongs to the paramagnetic ferroelectric phase. To our knowledge, this is the first reliable PES and XAS study on multiferroic samples¹⁸. This study provides the information on the electronic structures of RMnO_3 ($R=Y, \text{Er}$) in their ferroelectric and paramagnetic phases even though we did not perform the polarization-dependent spectroscopy measurement across T_E or T_N .

Polycrystalline RMnO_3 samples ($R=Y, \text{Er}$) were synthesized by using the standard solid-state reaction method. Cation oxides of R_2O_3 ($R=Y, \text{Er}$) (99.999%) and Mn_2O_3 (99.999%) were thoroughly mixed in order to achieve a homogeneous mixture. The mixed powders were heated to 900°C for 12 hours and later they were annealed at 1100°C for 24 hours and subsequently at 1200°C for 24 hours before final sintering at 1350°C for 24 hours with intermediate grindings. The purpose of intermediate grindings was to prevent the formation of impurity phases. The x-ray diffraction (XRD) measurements at room temperature showed that all the samples have a single hexagonal RMnO_3 phase.

Valence-band PES, O $1s$ XAS, and Mn $2p$ XAS measurements were performed at the 8A1 undulator beamline of the Pohang Accelerator Laboratory (PAL). Samples were cleaned *in situ* by repeated scraping with a diamond file and the data were obtained at room temperature with the pressure better than 4×10^{-10} Torr. The Fermi level E_F ¹⁹ and the overall instrumental resolution (FWHM) of the system were determined from the valence-band spectrum of a scraped Pd metal in electrical contact with a sample. The FWHM was about 100 – 400 meV between a photon energy $h\nu \sim 130$ eV and $h\nu \approx 600$ eV. All the spectra were normalized to the incident photon flux. The XAS spectra were obtained by employing the total electron yield method. The experimental energy resolution for the XAS data was set to ~ 100 meV at the O $1s$ and Mn $2p$ absorption thresholds ($h\nu \approx 500\text{-}600$ eV).

Figure 1 compares the Mn $2p$ XAS spectra of RMnO_3 ($R=Y, \text{Er}$) to those of reference Mn compounds having formal Mn valences of 3+ (Mn_2O_3 , reproduced from Ref.²⁰), 4+ (MnO_2 reproduced from Ref.²¹), 2+ (MnO reproduced from Ref.²¹), and that of Mn metal (reproduced from Ref.²²). The XAS data of MnO_2 , MnO , and Mn metal were shifted by -0.8 eV, $+1.0$ eV, and -1.3 eV, respectively, to allow for the better comparison of the data. It is well known that the peak positions and the line shape of the Mn $2p$ XAS spectrum depend on the local electronic structure of the Mn ion, so that the $2p$ XAS spectrum provides the information on the valence state of the Mn ion^{23,24}. Figure 1 shows clearly that the

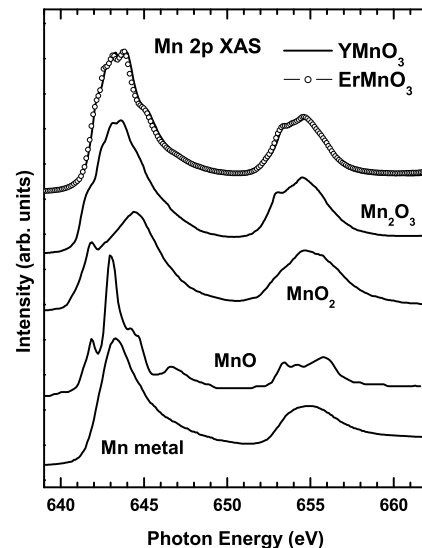


FIG. 1: Comparison of the Mn $2p$ XAS spectra of YMnO_3 (solid lines) and ErMnO_3 (symbols) to those of Mn_2O_3 (Mn^{3+}) [Ref.²⁰], MnO_2 (Mn^{3+}) [Ref.²¹], MnO (Mn^{2+}) [Ref.²¹], and Mn metal [Ref.²²].

Mn $2p$ XAS spectra of RMnO_3 ($R=Y, \text{Er}$) are essentially identical to each other, and that they are very similar to that of Mn_2O_3 . For comparison, they are quite different from those of MnO ($2+$), MnO_2 ($4+$), and Mn metal. This observation indicates that the valence states of Mn ions in RMnO_3 are nearly trivalent (Mn^{3+}), with the $3d^4$ configuration, but far from being divalent (Mn^{2+} , $3d^5$) or tetravalent (Mn^{4+} , $3d^3$). This finding is consistent with the finding of Mn K-edge XANES²⁵, and with the general consensus of Mn^{3+} ions in the ionic bonding picture for hexagonal RMnO_3 .

If Mn ions in RMnO_3 have the $3d^4$ configurations, then the next question would be which states are occupied which ones are unoccupied, and where these states are located with respect to E_F . In order to answer these questions, we have investigated the photoemission spectral weight distribution of the Mn $3d$ electrons, by employing resonant photoemission spectroscopy (RPES) near the Mn $2p \rightarrow 3d$ absorption threshold²⁷.

Top of Fig. 2 shows the valence-band RPES spectra of YMnO_3 near the Mn $2p_{3/2}$ absorption edge. We have also done RPES measurements for ErMnO_3 , but the valence-band PES spectra have large contribution from Er $4f$ electron emissions, which overlap with both Mn $3d$ and O $2p$ emissions. So we do not present the PES data for ErMnO_3 in this paper. The inset shows the Mn $2p_{3/2}$ XAS spectrum of YMnO_3 , and the arrows in the XAS spectrum represent $h\nu$'s where the valence-band spectra were obtained. The off-resonance valence-band PES spectrum (A) consists of both O $2p$ and Mn $3d$ electron emissions with comparable contributions, but has the negligible contribution from Y s/p electron emissions²⁶.

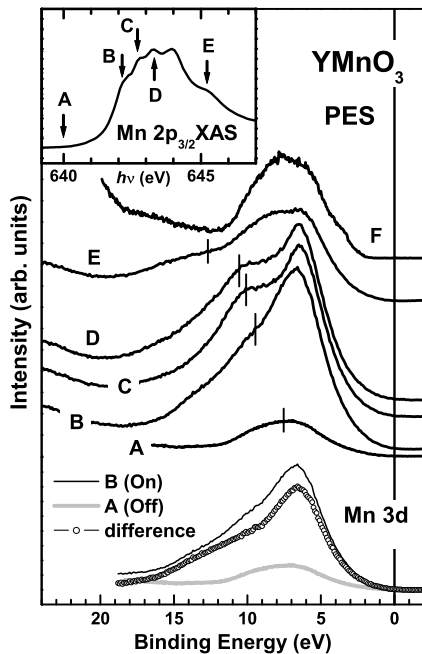


FIG. 2: Valence-band PES spectra of YMnO_3 near the $\text{Mn } 2p_{3/2} \rightarrow 3d$ absorption edge. Inset: The $\text{Mn } 2p_{3/2}$ XAS spectrum of YMnO_3 . Arrows denote $h\nu$'s where the valence-band PES spectra were obtained. Bottom: Comparison of the on-resonance (solid line) and off-resonance valence-band PES spectra (gray line) in $\text{Mn } 2p \rightarrow 3d$ RPES, and the difference between these two (open dots).

The valence-band PES spectrum, labeled as F , was obtained with $h\nu = 1486.6$ eV. This spectrum is very similar to the off-resonance spectrum (A), because, at $h\nu = 1486.6$ eV, the $\text{O } 2p$ and $\text{Mn } 3d$ electron emissions are also of comparable magnitudes²⁶. The enhanced features near ~ 7 eV binding energy at the $\text{Mn } 2p \rightarrow 3d$ absorption energy (B) represent the resonant $\text{Mn } 3d$ electron emission. Therefore the difference between the on-resonance and off-resonance spectra can be considered to represent the *bulk* $\text{Mn } 3d$ partial spectral weight (PSW) distribution²⁷. The vertical bars, marked for those features that shift away from E_F with increasing $h\nu$, denote the Mn LMM Auger emission that appears at a fixed kinetic energy (KE) of $\text{KE} \sim 635$ eV²⁸. These Auger peaks also reveal the intensity enhancement near the $\text{Mn } 2p$ absorption threshold. It is known that the transition-metal (T) Auger peaks show the resonant behavior near the $\text{T } 2p \rightarrow 3d$ RPES²⁹.

Bottom of Fig. 2 presents the extraction procedure of the $\text{Mn } 3d$ PSW for YMnO_3 . As a first approximation, it is taken as the difference between the $\text{Mn } 2p \rightarrow 3d$ on-resonance spectrum (solid line) and off-resonance spectrum (gray line). In this extraction procedure, we have used the on-resonance spectrum at B , instead of C or D , to reduce the effect of the Mn LMM Auger emission. The extracted $\text{Mn } 3d$ PSW exhibits a peak centered at ~ 7

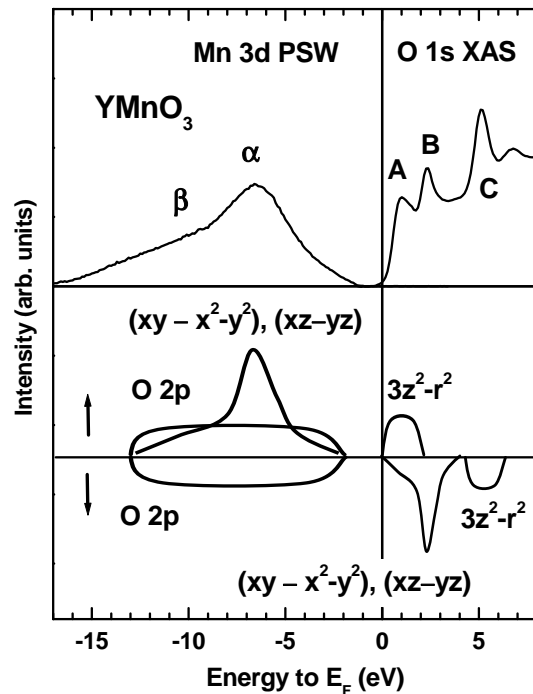


FIG. 3: Top: Combined $\text{Mn } 3d$ PSW and $\text{O } 1s$ XAS for YMnO_3 . Bottom: The schematic diagram for the $\text{Mn } 3d$ PDOS of YMnO_3 . \uparrow and \downarrow represent the majority- and minority-spin states, respectively.

eV binding energy with an asymmetric and long tail to the high binding energy side (up to ~ 15 eV). Part of this high binding tail is ascribed to the underlying Mn Auger peak. The extracted $\text{Mn } 3d$ PSW for YMnO_3 shows that $\text{Mn } 3d$ states are located well below E_F but that there is nearly no $\text{Mn } 3d$ occupied states near E_F . Note that both the off-resonance spectrum (A) and the $h\nu = 1486.6$ eV spectrum (F) represent the mixture of $\text{O } 2p$ and $\text{Mn } 3d$ emissions. Therefore the bottom part of Fig. 2 reveals that the occupied $\text{Mn } 3d$ states lie in the middle of the $\text{O } 2p$ states and that they overlap with the $\text{O } 2p$ states very much, implying the strong hybridization between $\text{Mn } 3d$ and $\text{O } 2p$ states.

Figure 3 shows the combined $\text{Mn } 3d$ PSW and the $\text{O } 1s$ XAS spectrum of YMnO_3 ³⁰. The $\text{O } 1s$ XAS spectrum represents the transition from the $\text{O } 1s$ core level to the unoccupied $\text{O } 2p$ states which are hybridized with the other electronic states, so it provides a reasonable estimate of the unoccupied conduction bands. The peaks A , B , C in the $\text{O } 1s$ XAS spectrum of YMnO_3 have also been observed in ErMnO_3 and they were very similar to each other, indicating that they have mainly the $\text{O } 2p$ - $\text{Mn } 3d$ character. At the bottom of Fig. 3, we also

provide a schematic diagram for the partial densities of states (PDOS) for YMnO_3 . We have determined this schematic PDOS diagram through the comparison of the PES/XAS data and the LSDA+ U (LSDA: local spin-density approximation, U : Coulomb interaction) band calculations for YMnO_3 ^{16,17}.

The features observed in the PES/XAS are ascribed to the following states. α : the occupied Mn 3*d* states consisting of the narrow ($d_{xz} \uparrow - d_{yz} \uparrow$) states, which are superposed on top of the rather broad ($d_{xy} \uparrow - d_{x^2-y^2} \uparrow$) states, β (the high binding energy shoulder to α): the Mn Auger peak, $\alpha + \beta$ (the broad valence-band PES features underneath the Mn 3*d* states): the O 2*p* states. Note that the occupied O 2*p* states are hybridized with ($d_{xy} - d_{x^2-y^2}$) states, consistent with the band-structure calculations^{16,17}. In the XAS side, the marked peaks represent the following states. *A*: the unoccupied Mn $d_{3z^2-r^2} \uparrow$ states, *B*: the unoccupied Mn ($d_{xy} \downarrow - d_{x^2-y^2} \downarrow$) and ($d_{xz} \downarrow - d_{yz} \downarrow$) states, *C*: the unoccupied Mn $d_{3z^2-r^2} \downarrow$ states. Thus the state just above E_F corresponds to Mn $d_{3z^2-r^2} \uparrow$, and so the trivalent Mn^{3+} ions in RMnO_3 are in the high-spin state ($S = 2$) with the configuration of ($d_{xz} \uparrow - d_{yz} \uparrow$)²($d_{xy} \uparrow - d_{x^2-y^2} \uparrow$)². Considering the uncertainty in the binding energy calibration of PES data¹⁹, the energy separation between the peak α in the valence-band PES and the peak *A* in the O 1*s* XAS amounts to $7 \sim 8$ eV, which gives a rough measure of $U + \Delta_{CF}$ (U : on-site Coulomb interaction between Mn 3*d* electrons, Δ_{CF} : the crystal-field splitting between $d_{3z^2-r^2}$ and $d_{xz} - d_{yz}$). Using $\Delta_{CF} \approx 2$ eV from the LSDA band structure calculation¹⁶, the estimated value of U would be of the order of $5 \sim 6$ eV. The energy separation (~ 2 eV) between the top of the valence band and the peak *A* in the O 1*s* XAS is expected to correspond to the lowest energy peak in the optical absorption spectrum for YMnO_3 ^{18,31}. We ascribe this energy separation to the energy difference between the occupied O 2*p* states, which are strongly hybridized to the ($d_{xy} \uparrow - d_{x^2-y^2} \uparrow$) states, and the unoccupied Mn $d_{3z^2-r^2} \uparrow$ states.

Note that the extracted Mn 3*d* PSW shows negligible spectral weight near E_F . Thus our schematic PDOS diagram shown in Fig. 3 implies that the topmost electronic

states in the valence bands of YMnO_3 (those closest to E_F) are mostly O 2*p* states. According to this picture, the lowest-energy optical transition would be the O *p*-Mn *d* transition, suggesting that YMnO_3 is likely to be a charge-transfer insulator. This picture is consistent with the electronic structures obtained by using the LSDA+ U , rather than those by the LSDA method¹⁶. The present data, however, indicate that the Mn 3*d* Coulomb interaction U is not as large as employed in Ref.¹⁶, $U = 8$ eV. Noteworthy is that our model for the electronic structure of YMnO_3 is different from that proposed based on the optical study of LuMnO_3 ¹³. They observed a sharp peak at 1.7 eV in the optical absorption spectrum for LuMnO_3 even at room temperature, which was ascribed to the on-site Mn *d*-*d* transition. In contrast, the similar absorption peaks were observed in RMnO_3 ($R = \text{Sc, Y, Er}$), which were interpreted as arising from charge transfer from O 2*p* to Mn 3*d* states³¹. The present PES/XAS data indicate that the latter interpretation is more consistent with the real electronic structures in RMnO_3 .

In conclusion, the electronic structures of hexagonal multiferroic RMnO_3 ($R = \text{Y, Er}$) materials have been investigated by employing Mn 2*p* \rightarrow 3*d* RPES, Mn 2*p* XAS, and O 1*s* XAS. The Mn 2*p* XAS spectra of RMnO_3 ($R = \text{Y, Er}$) show that Mn ions are in the formally trivalent Mn^{3+} states, implying the ($d_{xz} \uparrow - d_{yz} \uparrow$)²($d_{xy} \uparrow - d_{x^2-y^2} \uparrow$)² configurations with the total spin of $S = 2$ per Mn ion. According to Mn 2*p* \rightarrow 3*d* RPES for YMnO_3 , the occupied Mn ($d_{xz} - d_{yz}$) states lie very deep below E_F , with a peak around ~ 7 eV binding energy. The occupied Mn ($d_{xy} - d_{x^2-y^2}$) states overlap with the O 2*p* states very much, but show negligible Mn 3*d* spectral weight above the O 2*p* states, suggesting that YMnO_3 is likely to be a charge-transfer insulator. The lowest unoccupied peak in the O 1*s* XAS is ascribed to the unoccupied Mn $d_{3z^2-r^2}$ state. This finding is compatible with the recent structural studies of RMnO_3 ^{6,7}, which show tilting of MnO_5 blocks in their ferroelectric phases.

Acknowledgments— We thank S.-W. Cheong for helpful discussions. This work was supported by the KRF (KRF-2002-070-C00038) and by the KOSEF through the CSCMR at SNU and the eSSC at POSTECH. The PAL is supported by the MOST and POSCO in Korea.

* kangjs@catholic.ac.kr

¹ E. F. Bertaut, E. F. Forrat, and P. Fang, C. R. Acad. Sci. (Paris) **256**, 1958 (1963).

² H. L. Yakei, W. C. Koehler, E. F. Bertaut, E. F. Forrat, Acta Crystallogr. **16**, 957 (1963).

³ G. A. Smolenskii and I. E. Chupis, Sov. Phys. Usp. **25**, 475 (1982).

⁴ H. Schmid, Ferroelectrics **162**, 317 (1994).

⁵ W. C. Koehler, H. L. Yakei, E. O. Wollan, and J. W. Cable, Phys. Lett. **9**, 93 (1964).

⁶ T. Katsufuji, S. Mori, M. Masaki, Y. Moritomo, N. Yamamoto, and H. Takagi, Phys. Rev. B **64**, 104419 (2001).

⁷ B. B. van Aken, T. T. M. Palstra, A. Filippetti, and N. A. Spaldin, Nature Materials **3**, 164 (2004).

⁸ Z. J. Huang, Y. Cao, Y. Y. Sun, Y. Y. Xue, and C. W. Chu, Phys. Rev. B **56**, 2623 (1997).

⁹ N. Iwata and K. Kohn, J. Phys. Soc. Jpn. **67**, 3318 (1998).

¹⁰ T. Kimura, T. Goto, H. Shintani, K. Ishizaka, T. Arima, and Y. Tokura, Nature (London) **426**, 55 (2003).

¹¹ M. Fiebig, Th. Lottermoser, D. Fröhlich, A. V. Goltsev, and R. V. Pisarev, Nature (London) **419**, 818 (2002).

¹² T. Lottermoser, T. Lonkai, U. Amann, D. Hohlwein, J. Ihlinger, and M. Fiebig, Nature (London) **430**, 541 (2004).

¹³ A. B. Souchkov, J. R. Simpson, M. Quijada, H. Ishibashi,

- N. Hur, J. S. Ahn, S.-W. Cheong, A. J. Millis, and H. D. Drew, *Phys. Rev. Lett.* **91**, 027203 (2003).
- ¹⁴ N. A. Hill and A. Filippetti, *J. Magn. Magn. Mater.* **242-245**, 976 (2002).
- ¹⁵ N. A. Spandin and W. E. Pickett, *J. Solid State Chem.* **176**, 615 (2003).
- ¹⁶ J. E. Medvedeva, V. I. Anisimov, O. N. Mryasov, and A. J. Freeman, *J. Phys.: Condens. Matter* **12**, 4947 (2000).
- ¹⁷ M. Qian, J. Dong, and D. Y. Xing, *Phys. Rev. B* **63**, 155101 (2001).
- ¹⁸ W. C. Yi, S. I. Kwun, and J. G. Yoon, *J. Phys. Soc. Jpn.* **69**, 2706 (2000).
- ¹⁹ Since RMnO_3 samples are insulating, there is some ambiguity in determining E_F . However, no time-dependent charging effects were observed in the valence-band PES spectra of RMnO_3 . Therefore the absolute values of binding energies do not have much meaning in these data, but the relative energy separations are meaningful.
- ²⁰ P. Ghigna, A. Campana, A. Lascialfari, A. Caneschi, D. Gatteschi, A. Tagliaferri, and F. Borgatti, *Phys. Rev. B* **64**, 132413 (2001).
- ²¹ C. Mitra, Z. Hu, P. Raychaudhuri, S. Wirth, S. I. Csiszar, H. H. Hsieh, H.-J. Lin, C. T. Chen, and L. H. Tjeng, *Phys. Rev. B* **67**, 92404 (2003).
- ²² Y. Yonamoto, T. Yokoyama, K. Amemiya, D. Matsumura, and T. Ohta, *Phys. Rev. B* **63**, 214406 (2001).
- ²³ F. M. F. de Groot, J. C. Fuggle, B. T. Thole, and G. A. Sawatzky, *Phys. Rev. B* **42**, 5459 (1990).
- ²⁴ G. van der Laan and I. W. Kirkman, *J. Phys.: Condens. Matter* **4**, 4189 (1992).
- ²⁵ C. T. Wu, Y. Y. Hsu, B. N. Lin, and H. C. Ku, *Physica B* **329-333**, 709 (2003).
- ²⁶ J. J. Yeh and I. Lindau, *At. Data Nucl. Data Tables* **32**, 1 (1985), where calculated atomic photoionization cross sections are given.
- ²⁷ J.-S. Kang, J. H. Kim, A. Sekiyama, S. Kasai, S. Suga, S. W. Han, K. H. Kim, T. Muro, Y. Saitoh, C. Hwang, C. G. Olson, B. J. Park, B. W. Lee, J. H. Shim, J. H. Park, and B. I. Min, *Phys. Rev. B* **66**, 113105 (2002).
- ²⁸ Handbook of Auger Electron Spectroscopy, edited by C. L. Herdberg, Third Edition (Physical Electronics, Inc., Minnesota (1995).
- ²⁹ J.-S. Kang, J. H. Kim, A. Sekiyama, S. Kasai, S. Suga, S. W. Han, K. H. Kim, E. J. Choi, T. Kimura, T. Muro, Y. Saitoh, C. G. Olson, J. H. Shim, and B. I. Min, *Phys. Rev. B* **68**, 012410 (2003).
- ³⁰ In this comparison, the inelastic background has been subtracted in the Mn $3d$ PSW, and the O $1s$ XAS spectrum has been shifted by -530 eV by referring to the optical gap size of YMnO_3 .
- ³¹ A. M. Kalashnikova and R. V. Pisarev, *JETP Lett.* **78**, 143 (2003).